J. CHEM. SOC. FARADAY TRANS., 1990, 86(19), 3173–3180

The Bruker Lecture
Modern Techniques in Electron Paramagnetic Resonance Spectroscopy†

Jack H. Freed
Baker Laboratory of Chemistry, Cornell University, Ithaca, NY 14853-1301, USA

The last few years have seen important new advances in EPR which have the possibility of revolutionizing the applications of EPR in chemistry and related fields. New methods include (*a*) two-dimensional and Fourier-transform EPR; (*b*) far-infrared EPR (with 1 mm waves); (*c*) dynamic imaging of diffusion by EPR; (*d*) powerful computational algorithms for spectral simulation. These new methods and their implications for chemical research are discussed.

1. Introduction

There have been several significant developments in EPR techniques in the past five to eight years. We note first of all the development of two-dimensional Fourier-transform (2D-FT) EPR and its initial applications to the study of molecular dynamics in liquids.[1–6] The motivation for this development came, in part, from our recent work on field-swept two-dimensional electron-spin-echo (2D-ESE) methods.[5–10] The new 2D-FT-EPR experiment considerably enhances the resolution and range of EPR for studying molecular dynamics, and it should also lead to improved structural studies by EPR. It holds the potential for revolutionizing EPR by analogy to the way FT and 2D methods have revolutionized NMR.

A second key development has been high-field and high-frequency EPR. This includes our 1 mm wave EPR spectrometer and its initial application to studies of motional dynamics.[11,12] This spectrometer is the first high-resolution EPR spectrometer based on far-infrared (FIR) technology. The advantages of high-frequency EPR include: (1) greater resolution for polycrystalline spectra; (2) greater sensitivity to faster motional dynamics; (3) extension of the range of slow-motional EPR studies to fast motion; (4) potentially greater signal sensitivity.

Another key development has been EPR imaging. Our efforts have been directed to an accurate and convenient method to measure translational diffusion coefficients, D, of radicals and spin labels in isotropic and oriented fluids.[13–16] This method, dynamic imaging of diffusion (DID) by EPR, is successful in measuring D over a very wide range: $10^{-9} \leqslant D/\mathrm{cm^2\ s^{-1}} \leqslant 10^{-5}$.

Finally, we note the development of highly sophisticated computational algorithms for calculating slow motional c.w. and 2D-EPR spectra.[17,18] This has led to a rapid and easy-to-use slow motional EPR program that has been made generally available in diskette form for IBM-PC compatible computers.[19] It also permits non-linear least-squares fitting of slow motional spectra.

We describe these developments below.

2. Two-Dimensional Electron-spin Echoes (2D-ESE)

One of the fundamental problems in the use of c.w. EPR in motional studies has been its relative insensitivity to slow motions, *e.g.* for rotational correlations times $\tau_R > 10^{-7}$ s the EPR spectrum of nitroxide probes or spin labels yields a broad inhomogeneous rigid-limit pattern. However, a particular advantage of the spin-echo experiment over c.w. techniques is that the timescale of the echo experiment is just T_2, the inverse of the homogeneous linewidth, which in slow-motional spectra, is much longer than the inverse of the inhomogeneous linewidth (usually called T_2^*) affecting the c.w. spectrum[20] It is the homogeneous T_2 that is sensitive to the motions. This means that slower motions can be detected by echo methods than by c.w. EPR. In order to maximize the information obtained from studying T_2, we have introduced a field-swept 2D-ESE technique which provides a simple map of the homogeneous T_2 across the spectrum. In studies in viscous liquids,[7] on surfaces,[10] in oriented model membranes,[21] and spin-labelled macromolecules,[22] we have shown that these 'T_2-plots' are not only very sensitive to motion in the region $10^{-7} < \tau_R/\mathrm{s} < 10^{-4}$, but also to the motional models used to describe molecular rotational reorientation. This provides clear distinctions between models of Brownian *vs.* jump diffusion just from the patterns of the 'T_2-plots'.[7,23] It also provides clear distinctions of isotropic *vs.* anisotropic motions as well as the extent of ordering in oriented fluids.[23]

Slow-motional dynamics can also be studied in the domain of T_1-type experiments. In the past, c.w. techniques such as saturation-EPR,[24,25] saturation-transfer EPR[26] and ELDOR[27] have been used. More recently, time-domain techniques of ELDOR spin-echoes[28,29] and saturation-recovery[30,31] have been employed. Our theory for the study of motional dynamics by the T_1-type inversion-recovery (IR) and stimulated echo (SE) sequences, showed that in general, the rate of magnetization transfer (MT) out of each spectral region should vary across the spectrum in a way that could be more sensitive to molecular motion than the T_2-type experiment described above.[9,32] We developed a field-swept 2D-ESE MT experiment that is based upon the SE pulse sequence.[9] It will, in general, lead to a sum of exponential decays which can be fitted, to a good approximation, by a sum of just two: the decay in $T_1 = (2W_e)^{-1}$, where W_e is the electron-spin-flip rate, and the decay in T_A, the 'MT relaxation time', and it is of order of τ_R. The experiment was demonstrated in a study on NO_2 adsorbed on crushed Vycor, and it showed dramatic evidence for the model of very anisotropic rotation of the NO_2 on the surface.[9,10] It appears that rotatonal motions are detectable at lower temperatures than with T_2-type 2D-ESE experiments.

3. Two-Dimensional Fourier-transform EPR (2D-FT-EPR)

A major limitation of the field-swept methods is the long data-acquisition periods required, because one sweeps the field

† The fifth Bruker Lecture of the Royal Society of Chemistry given at the 23rd Annual International ESR Conference held at Royal Holloway and Bedford New College, University of London, on 26–30 March, 1990.

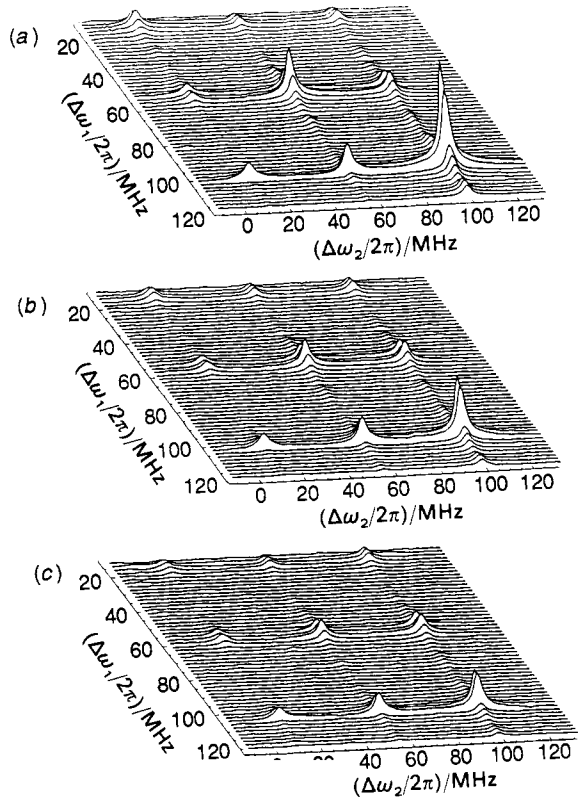

Fig. 1. 2D-ELDOR spectra obtained for a 0.5 mmol dm^{-3} solution of the nitroxide radical MOTA in the nematic phase of liquid crystal 40,7 at 60 °C for different mixing times, T: (*a*) 200 ns, (*b*) 400 ns, (*c*) 600 ns. They show how the relative importance of the cross-peaks compared to the auto-peaks increases with T due to exchange processes even as the overall 2D spectrum ultimately decays away as T/T_1 becomes large. The six cross-peaks in this example represent exchange arising from both Heisenberg exchange and nuclear spin-flips induced by electron–nuclear dipolar interactions. [MOTA is 4-methylamino-2,2′-6,6′-tetramethylpiperidine N-oxide (perdeuterated) and 40,7 is *N*-(*p*-butoxybenzylidene)-*p*-n- heptylaniline].

through the spectrum, collecting the echo envelope decay at each spectral position. If instead, one were to irradiate the entire spectrum and collect the entire FID (or the echo shape) with each pulse sequence, one could expect to realize much more rapid data acquisition. Such ideas are by analogy to NMR where FT and 2D-FT methods have been well developed. However, FT-EPR offered major instrumental challenges compared to FT-NMR. First, the timescale of electron-spin relaxation is of the order of ns (compared to ms for NMR). Secondly, an EPR spectrum, such as that of a (motionally narrowed) nitroxide, covers *ca.* 100 MHz, requiring time resolution of the order of at least 10 ns (with quadrature detection) and narrow intense pulses. Finally, microwave technology is more complex than the equivalent r.f. technology.

We have now extensively developed both FT and 2D-FT EPR techniques in our laboratory.[1–6] Related FT-EPR techniques have also been developed at Argonne Labs by Bowman and co-workers.[33] A number of instrumental innovations were required to enable these experiments to be performed. They include the use and interfacing of fast (ns) transient digitizers and a microwave quadrature detector, the development of a special anode modulator to rapidly switch the high-power TWT amplifier,[3,6] and most recently the development of special bridged loop–gap resonators (BLGR)[34] and composite pulse techniques.[34] The anode modulator leads to significantly reduced dead times in both t_1 and t_2 due to rapid turn-off of the TWT amplifier. The BLGR allows us to obtain large microwave magnetic fields (needed for spectral coverage) with very low resonator Q (needed for bandwidths) and careful adjustment of resonator frequency. Composite pulses enhance spectral coverage. Also, sophisticated phase-cycling sequences are utilized to improve image rejection in the FT and to cancel unwanted axial and transverse peaks. New 2D data-processing methods based upon linear prediction were developed to enhance S/N and to remove various experimental artifacts.[3] The instrumental and data-processing developments have been reviewed.[5,6]

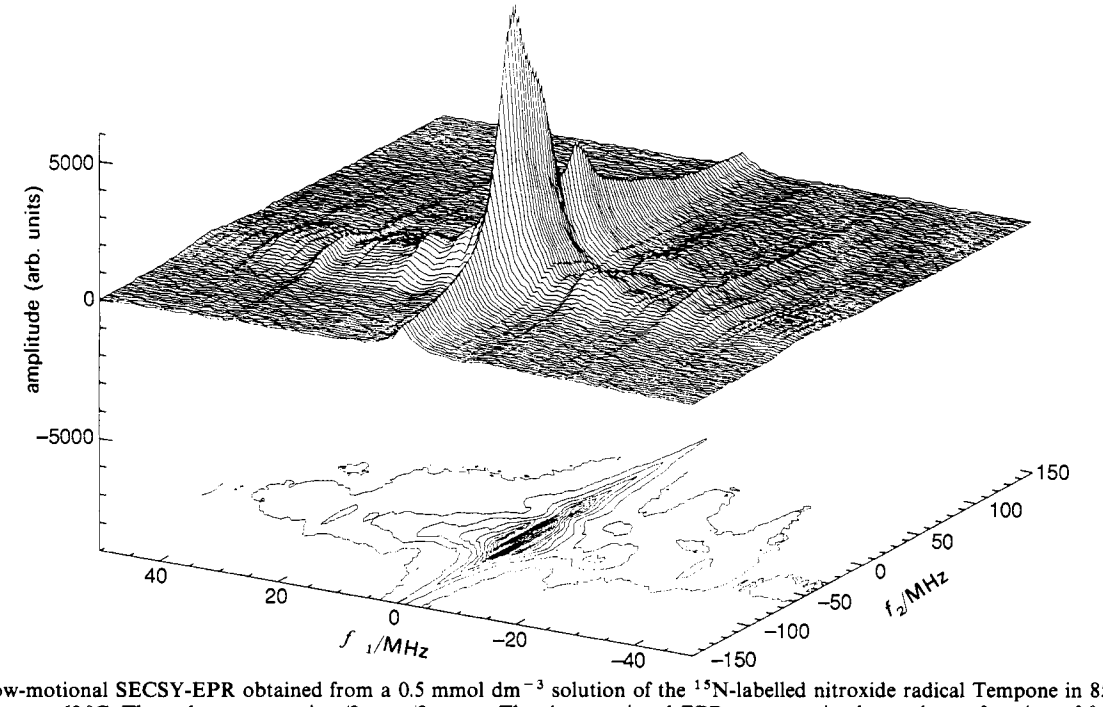

Fig. 2. Slow-motional SECSY-EPR obtained from a 0.5 mmol dm^{-3} solution of the ^{15}N-labelled nitroxide radical Tempone in 85% glycerol–15% water at −60 °C. The pulse sequence is $\pi/2$–t_1–$\pi/2$–t_1–t_2. The slow-motional EPR spectrum is observed as a function of f_2, whereas its homogeneous lineshape appears along frequency f_1. Additional satellite peaks along f_1 are due to nuclear modulation from the protons on Tempone (2,2′,6,6′-tetramethyl-4-piperidine *N*-oxide).

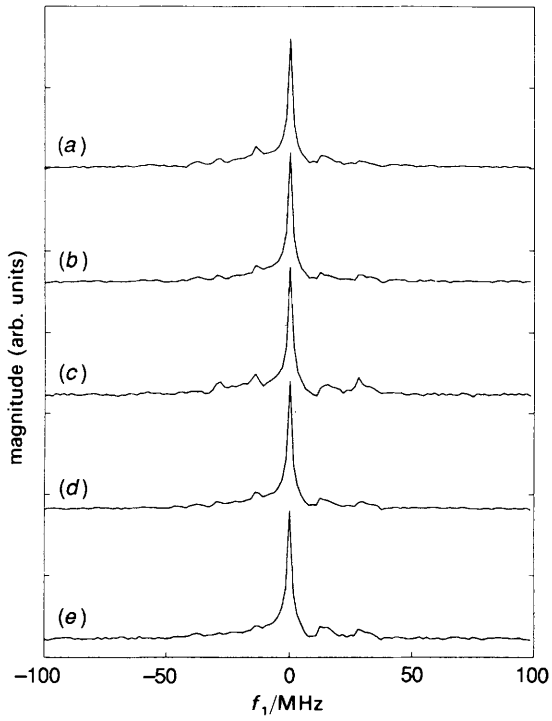

Fig. 3. Slices from the slow-motional (two-pulse) SECSY-EPR spectrum obtained from a 0.5 mmol dm^{-3} solution of the ^{15}N-labelled nitroxide radical Tempone in 85% glycerol–15% water at −90 °C. They show the projections along f_1 for different values of f_2 (MHz): (*a*) −65, (*b*) −40, (*c*) −15, (*d*) 10, (*e*) 35. They illustrate how the nuclear modulation satellite peaks vary with EPR spectral position.

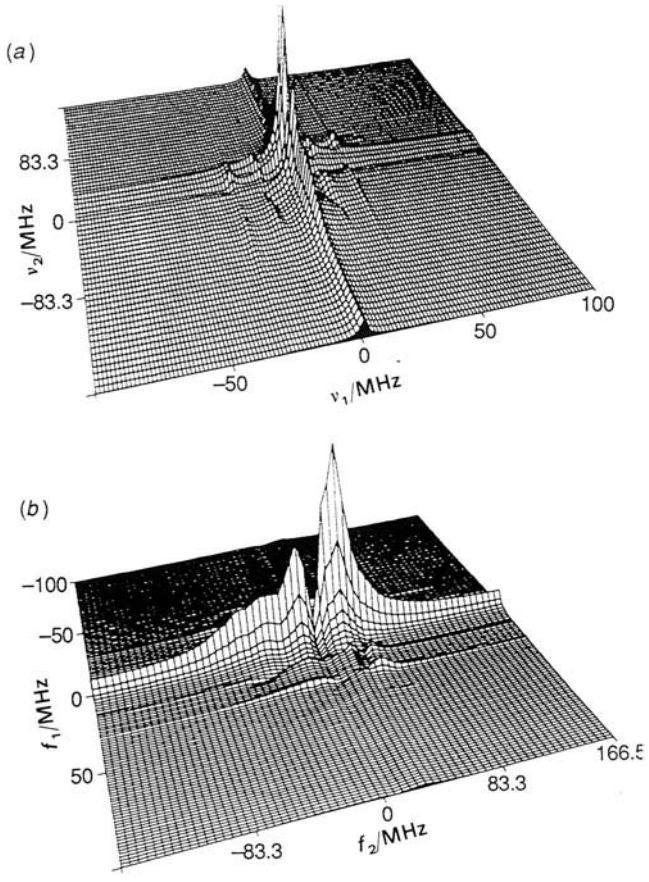

Fig. 4. Simulation of SECSY-EPR spectrum for a ^{15}N-labelled nitroxide with 12 completely equivalent methyl protons in the rigid limit of a polycrystalline sample. The two figures are equivalent but represent different viewing orientations. (Note that f_1 and f_2 in the simulations are opposite in sign convention to that used in fig. 2 and 3.) In this figure all the hf tensors are taken to be collinear with that of the *g*-tensor. We have used typical values for the ^{15}N tensor and *g*-tensor [*cf.* ref. (35)] with $\bar{a}_H = -1.2$ MHz, $(A_{\parallel} - A_{\perp}) = -9.3$ MHz and $\nu_H = 14.0$ MHz for the protons.

We initially succeeded with a range of 2D-EPR experiments on motionally narrowed nitroxides (spectral width of 100 MHz). We showed how the T_2-type of 2D-ESE experiment may be performed in a 2D-FT-EPR format as a SECSY-EPR (stimulated echo coherent spectroscopy by analogy to 2D-NMR).[8] We have demonstrated COSY-EPR (coherent spectroscopy)[2] which we expect will become important in EPR structural studies utilizing nuclear modulation.[3,5] It may be regarded as a correlation diagram of the spin system with auto and cross-peaks appearing as diagonal and off-diagonal peaks, respectively.

Most important, so far, was the development of 2D-FT-ELDOR (electron–electron double resonance), which is performed with only a single (coherent) frequency source.[1–6] It is based upon the Jeener–Ernst 2D pulse sequence originally developed in NMR.[3,6] In this technique, off-diagonal, or cross-peaks appear, which are a measure of magnetization transfer by spin-relaxation processes. These are, in fact, the 'ELDOR peaks' which are frequency-discriminated from the main or diagonal peaks. The principal spin-relaxation mechanisms are Heisenberg exchange (HE) which reports on bimolecular collision rates of radicals, and intramolecular electron–nuclear dipolar (END) interactions leading to nuclear spin-flip transitions (with rate W_n) which reflect rotational reorientation. The actual pattern of the cross-peaks helps to distinguish which relaxation mechanism is dominant.[2,4] In fig. 1 we illustrate such spectra wherein both HE and END mechanisms are contributing.

The quantitative accuracy of these experiments was demonstrated in a study of HE.[2] In an extensive study of a nitroxide probe in a liquid-crystalline medium combining T_2 measurements by ESE and measurements of W_n by 2D-ELDOR we have shown that we obtain (and isolate) a number of key spectral densities.[4] These spectral densities, studied as a function of angle of tilt of the liquid crystal with respect to the applied magnetic field, provide a wealth of information for studying molecular dynamics. The study we performed provided extensive data to rule out most simple models of reorientational dynamics in ordered fluids. Only a model involving coupled rotational and translational diffusion *via* a roto-translational potential was found to be consistent with our data.

Very recently we have succeeded in performing 2D-FT EPR in the slow-motional regime for a ^{15}N-labelled nitroxide. This requires the irradiation of spectral widths of *ca.* 200 MHz. The BLGR was particularly important in this application as was the use of special phase cycles. The spectra are of two types. The first is the basic SECSY experiment, utilizing the 2 pulses: $\pi/2$–t_1–$\pi/2$–t_1–t_2 with Fourier transformation in both t_1 and t_2. It is the FT version of the field-swept 'T_2-type' 2D-ESE experiment described in section 2. A typical 2D spectrum is shown in fig. 2. First we note that this 2D-FT spectrum was obtained in much shorter time, *ca.* an order of magnitude less than the field-swept variety. Secondly, we note, that because intense microwave fields are utilized, the nuclear modulation from the protons of Tempone leads to additional small peaks displaced from the main peak. Furthermore, these peaks are dependent on the EPR spectral position (*i.e.* ω_2), as shown in fig. 3. These observations are in good agreement with theoretical predictions illustrated in fig. 4 and 5. They show that SECSY-EPR would be applicable

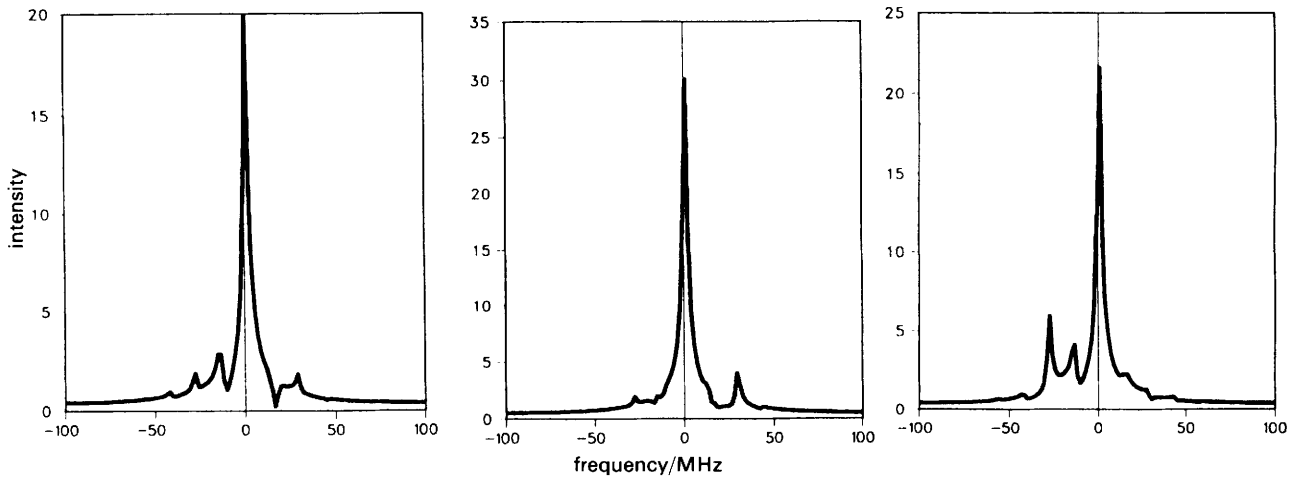

Fig. 5. Slices from the simulated SECSY-EPR spectrum in fig. 4. They show the projections along f_1 for different values of f_2 of -36, 36 and 10 MHz (from left to right). They illustrate how the nuclear modulation satellite peaks vary with EPR spectral position for the theoretical model of 12 completely equivalent methyl protons.

not only to studies of molecular dynamics, but also to structural studies from the nuclear modulation.

The second type of 2D-FT EPR in the slow-motional regime is a three-pulse SECSY experiment: $\pi/2$–t_1–$\pi/2$–T–$\pi/2$–t_1–t_2 with Fourier transformation in both T and t_2. It is the FT version of the field-swept 'MT type' experiments described in section 2. Although this 2D-FT spectrum will, in general, include effects from nuclear modulation, it is possible to tune at least some of them out by adjusting t_1.[35] This has been done in fig. 6. We have also performed this three pulse SECSY experiment but with T constant and t_1 varied, followed by FT in t_1 and t_2. This is a form of 2D ELDOR that gives rise to motional cross-peaks due to magnetization transfer in the slow-motional regime.

4. Far-infrared EPR

One of the most important advances in NMR has been the extension to high frequencies, requiring the use of superconducting magnets. This has provided large enhancements in sensitivity and spectral resolution, greatly broadening the utility of NMR. The effort towards higher EPR fields and frequencies was initially pioneered in the Soviet Union by Lebedev[37] who uses a spectrometer working at $\lambda = 2$ mm (*i.e.* 148 GHz) and 5.3 T fields based on microwave technology. In studies of nitroxide probes, they emphasized the significant advantages of high resolution for determining g tensors and studying molecular dynamics in the slow-motional regime. The sensitivity at 148 GHz is also reported to be significantly better than that of conventional EPR spectrometers.

Theoretically, even greater enhancement in sensitivity and resolution should be realized at still higher frequencies. However, it becomes increasingly difficult to utilize standard microwave technology at frequencies higher than 150 GHz. We have developed a new EPR spectrometer at $\lambda = 1.2$ mm (250 GHz) and 9 T fields that takes advantage of far-infrared technology based upon the principles of Gaussian optics.[11,12] We employ a special solid-state source that is phase locked

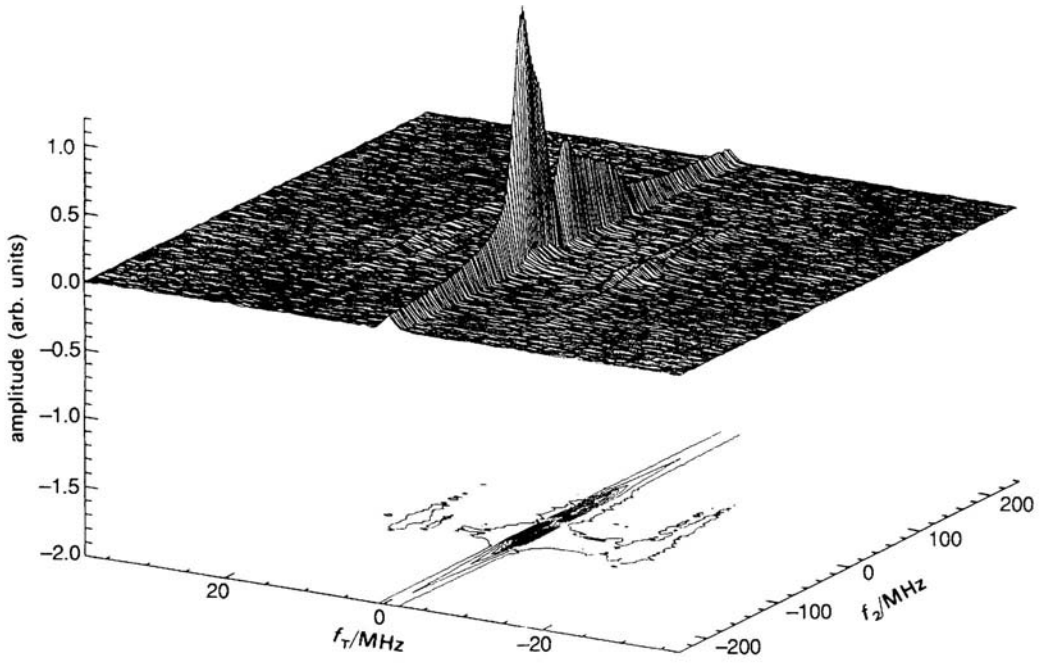

Fig. 6. Slow-motional SECSY-like-EPR spectrum obtained from the three-pulse sequence: $\pi/2$–t_1–$\pi/2$–T–$\pi/2$–t_1–t_2, where t_1 is held fixed and the mixing time T is varied. It is from a 0.5 mmol dm^{-3} solution of Tempone in 85% glycerol–15% water at -80 °C. The slow-motional EPR spectrum is observed as a function of f_2, whereas its T_1 and magnetization transfer rates appear along f_T. Additional satellite peaks along f_T due to proton-nuclear modulation have been largely suppressed by adjusting t_1.

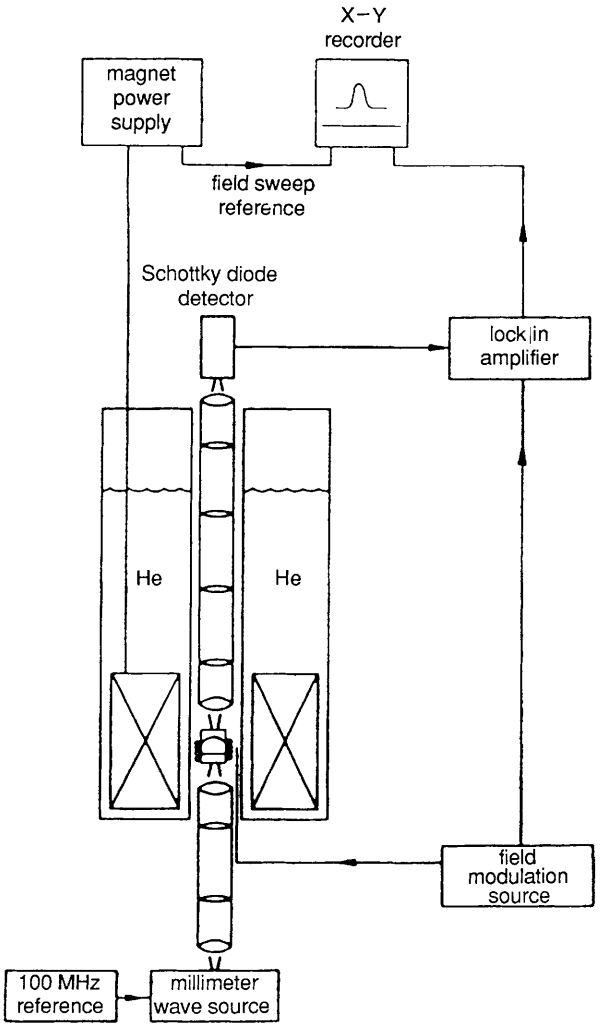

Fig. 7. Schematic of FIR EPR spectrometer. A phase-locked oscillator supplies 5 dBm c.w. at 250 GHz (1.2 mm) in a travelling wave of Gaussian profile. The travelling wave is refocussed by a Gaussian optics telescope, the FIR analogue of a periodic waveguide. The sample is placed in a low-Q, semi-confocal, Fabry–Pérot resonator in the region of highest homogeneity of the 9 T superconducting solenoid. The field may be swept ± 50 mT, by an auxiliary set of superconducting coils, designed to minimize coupling to the main coil.

The transmitted power is monitored by a room-temperature GaAs, Schottky diode. During a magnet sweep, the field is modulated so that a first-derivative transmission spectrum is obtained. The EPR resonance signal is rectified to a video band signal at the field modulation frequency and subsequently detected with a lock-in amplifier which uses the field-modulation frequency as the reference. After lock-in detection, the signal is displayed on an x–y recorder and subsequently digitized by a PC for further manipulation and analysis. The PC (not shown) also controls the magnet sweep under operator control.

and tripled to supply a very stable 1 mm signal. The 1 mm beam travels from the source, through a series of lenses to a low-Q Fabry–Perot resonator operating in the transmission mode. The spectromer is quite easy to operate. In fact, its operation is in a number of ways very similar to a conventional 9 GHz EPR spectrometer once the superconducting magnet is brought up to full value near resonance. A second smaller superconducting magnet is then utilized for field sweeps (*cf.* fig. 7).

We have demonstrated its great resolution in rigid-limit spectra from nitroxides. The g tensor components can be 'read' directly from the spectrum, and the hyperfine components are also easily obtained.[12] The fast through slow-motional and rigid-limit spectra are shown in fig. 8 and 9.

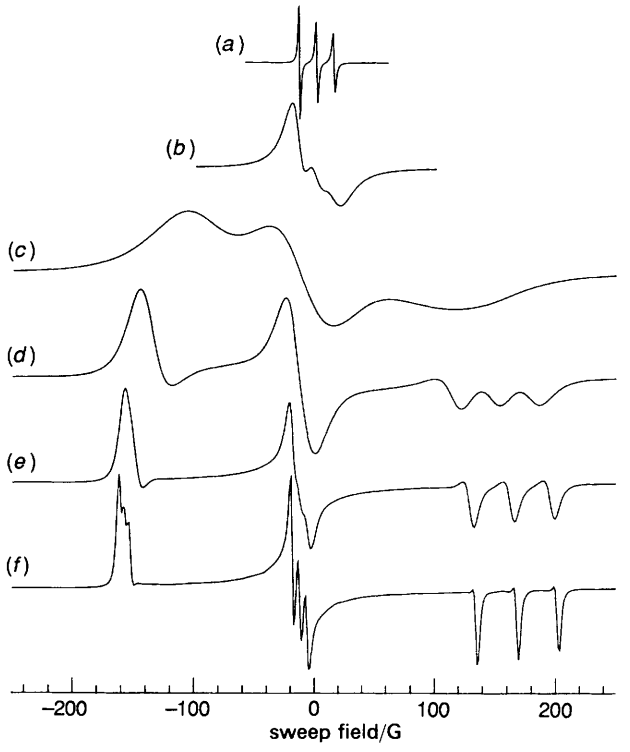

Fig. 8. Spectral simulations of PDT with toluene-d8 for 250 GHz EPR. We show fast-motional to rigid limit spectral simulations spanning five orders of magnitude in rotational correlation time τ_R/s: (*a*) 1×10^{-11}, (*b*) 1×10^{-10}, (*c*) 1×10^{-9}, (*d*) 1×10^{-8}, (*e*) 1×10^{-7}, (*f*) 1×10^{-5}. At 250 GHz, the spectral extent is dominated by g-tensor contributions in the slow-motional and rigid-limit regimes. One may simply read off the g values from the rigid-limit spectrum. At X-band, careful simulation is required to extract the g and A tensors in favourable cases.

We have clearly demonstrated that the 250 GHz spectra are much more sensitive to rotational motion in the fast-motional regime of $\tau_R < 10^{-10}$ s (for nitroxides).[11,12] This is due to the g-tensor contribution to the linewidth that depends quadratically on the magnetic field. We show in fig. 10 a comparative study of spin relaxation obtained at 250 GHz *vs.* 9 GHz, for a spin probe in an isotropic liquid to attempt to answer fundamental questions about the frequency dependence of spin relaxation.

A very important feature of such studies is that the slow-motional regime sets in for τ_R values an order of magnitude faster in the case of 250 GHz EPR *vs.* 9 GHz EPR. One is therefore able to combine the advantages of fast *vs.* slow-motional spin relaxation in a variety of systems by such comparative studies.

5. Dynamic Imaging of Diffusion (DID) by EPR *vs.* Heisenberg Exchange

DID-EPR has now been developed into a very accurate and relatively convenient method of measuring tracer translational diffusion coefficients, D.[13–16] In this method substantial linear field gradients are used along with well designed samples with inhomogeneous distributions of spins, and a special Fourier-space analysis.[14] We have obtained the D values of nitroxide probes in isotropic liquids, liquid crystals and model membranes. In the case of liquid crystals, one can measure the anisotropy of the diffusion tensor. The accuracy of this method, such as in measuring small differences in D, is illustrated in fig. 11. In studies on model membranes, we have

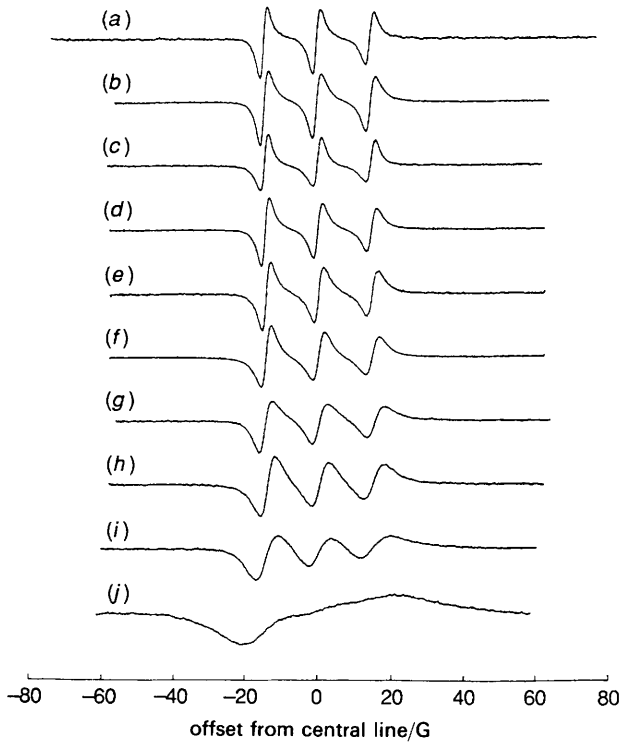

Fig. 9. Fast- to slow-motional 250 GHz EPR spectra. We show examples of fast-to slow-motional spectra of perdeuterated Tempone spin probe in toluene-d8. These spectra demonstrate the sensitivity of FIR-EPR to molecular reorientations over approximately a decade of rotational correlation times.

	rotational correlation time/ps	T/K
(*a*)	5.4	289
(*b*)	5.9	284
(*c*)	6.8	276
(*d*)	8.6	264
(*e*)	11	253
(*f*)	14	242
(*g*)	19	233
(*h*)	25	224
(*i*)	37	213
(*j*)	93	193

shown how the effects on D of varying the composition can be rationalized in terms of a free-volume model.[38]

Note that DID-EPR measures macroscopic D values (diffusive lengths *ca.* 100 μm), whereas Heisenberg exchange (HE) measures relative diffusion rates over molecular dimensions (*ca.* 100 Å). In a study of HE in liquid crystals,[39] our comparison with the D_{macro} obtained from DID-EPR showed that D_{micro} is generally several times larger. In the study of HE, it was also possible to obtain an independent estimate of D_{micro} from the intermolecular electron–electron dipolar (EED) interaction contributions to T_2. In general, we found that the values of D_{micro} obtained from the EED relaxation were 2–4 times larger than those obtained from HE. A similar observation had previously been reported for isotropic fluids.[40] We have provided an interpretation for this in terms of the effects of the pair-correlation function on the relative translational diffusion.[39] Our results suggest that solvent molecules inhibit collisons of radicals due to solvent structure about the radicals. Our explanation has yet to include the observed discrepancies between D_{macro} and D_{micro} obtained from HE. This work also pointed up the need to study accurately HE by the new methods of 2D ELDOR and ESE. These methods would also permit one to separate the HE contribution from those of the EED interactions.

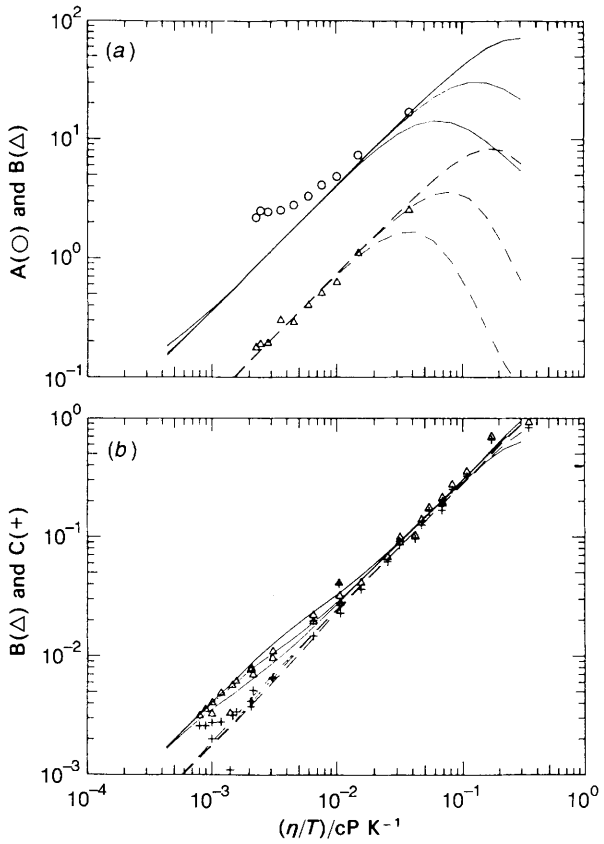

Fig. 10. Comparison of X-band[45] (*b*) and 250 GHz (*a*) linewidths for fast-motional spectra from perdeuterated Tempone in toluene-d8. One may write the linewidths in the form: $T_2^{-1}(M_I) = A + BM_I + CM_I^2$. At X-band, B and C may be well fitted and provide a measure of model-discrimination in the fast-motional limit. Work at 250 GHz indicates that A and B are the sensitive parameters and provide enhanced model discrimination in the fast-motional regime. [The additional high-temperature contribution to A is due to a line-broadening from residual O_2.] The 250 GHz results in (*a*) support the previous analysis[45] of the x-band results (*b*) in terms of the fluctuating torque model, wherein the spectral densities are modified by the parameter ε. The upper curves are for $\varepsilon = 1$ corresponding to the standard Debye form; lower curves: $\varepsilon = 25$; middle curves: $\varepsilon = 5.4$ representing the best fit to x-band data.

6. Theoretical and Computational Methods

Several years ago we developed the Lanczos algorithm (LA) as a very powerful and efficient method for computing slow-motional EPR spectra.[18,41,42] It leads to one to two orders of magnitude reduction in computation time and reduced storage requirements, yet it yields spectra to a high degree of accuracy. It is also appropriate for the general class of Fokker–Planck equations, and, in fact, there is a close connection between the LA with its recursive steps and the Mori projection scheme in statistical mechanics.[18,43]

Our 2D-ESE techniques have placed greater demands on the accuracy and convergence of theoretical simulations. This made evident several limitations in the existing LA.[18] We succeeded in overcoming all these limitations by blending the conjugate gradient method (CGM) with the LA for complex symmetric matrices.[17,18] Because of the power and reliability of this 'turbo-Lanczos' algorithm, it was possible first to produce a very compact slow-motional EPR (and NMR) computer program, that is now generally available to all

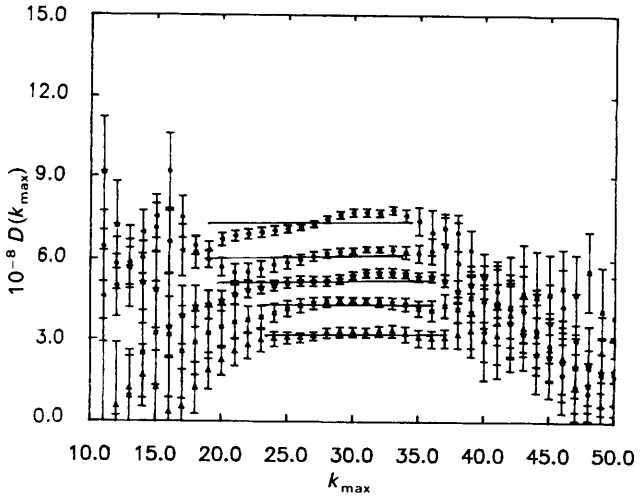

Fig. 11. The Fourier space analysis of DID-EPR for the translational diffusion coefficient, $D_\perp$ of the spin probe cholestane in the smectic liquid crystal blend 'S2' at several temperatures. $D_\perp$ refers to diffusion within the smectic plane. The Fourier space analysis gives $D_\perp$ ($cm^2\ s^{-1}$) *vs.* the maximum cut-off value of k (the Fourier transform of x, the position). Convergence is obtained for those k_{max} (cm^{-1}) which give a plateau value in $D_\perp$ and with minimum standard deviations shown as error bars [*cf.* ref. (15)]. The results are shown for temperatures 12.4 °C (▲), 15.8 °C (×), 19.2 °C (*), 22.4 °C, (●) and 25.7 (▲) (the horizontal lines show the plateau values). This result emphasizes the accuracy of DID-EPR so that small changes in D with temperature are clearly determined.

users,[19] as noted in section 1. Secondly, it has made it practical to implement (on the Cornell National Supercomputer) non-linear least-squares fitting of slow-motional EPR spectra even though such an algorithm (*e.g.* Levenberg–Marquardt) requires the simulation of 100–150 spectra (each involving 'diagonalization' of matrices of dimension 10^2–10^4) as it iterates to convergence.[44] This has greatly increased the accuracy and reliability of spectral fits to motional models

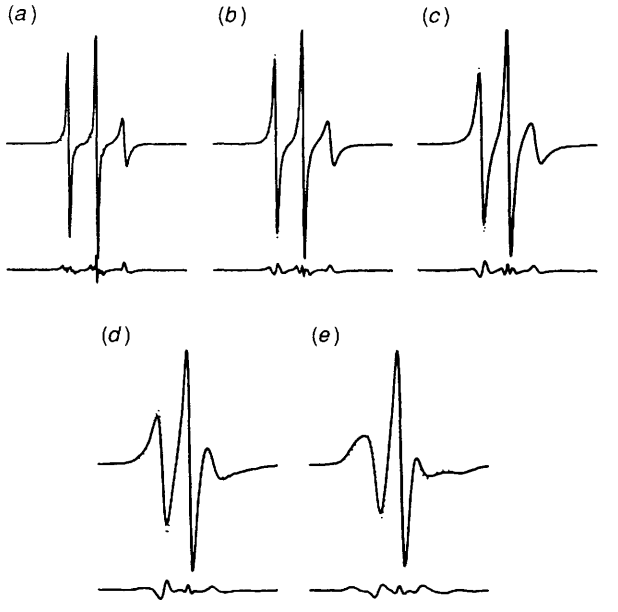

Fig. 12. Experimental (solid) and simulated (dotted) slow-motional EPR spectra of PD–Tempone in 85% glycerol-d_3–15% D_2O solvent at different temperatures: (*a*) 287.7 K, (*b*) 282.5 K, (*c*) 276.0 K, (*d*) 270.6 K, (*e*) 265.5 K. All these spectra were simultaneously fitted, by non-linear least squares, to a common Brownian diffusion model to yield an activation energy of 12.80 ± 0.02 kcal mol^{-1}. The line below each spectrum is the residue.

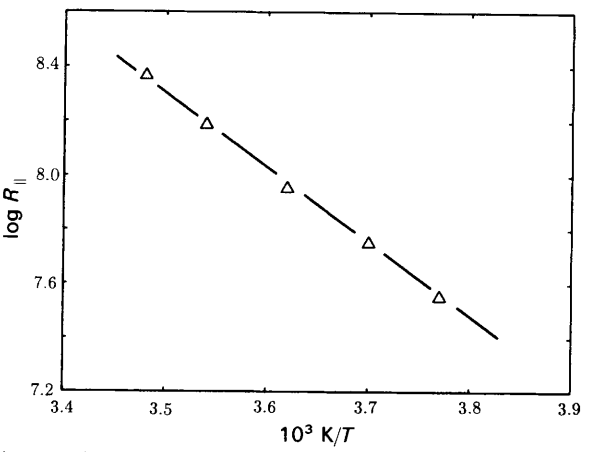

Fig. 13. The logarithm of the best-fit values of rotational diffusion tensor component $R_\parallel$ obtained from the non-linear least-squares fitting of EPR spectra of PD–Tempone in 85% glycerol-d_3–15% D_2O *vs.* the reciprocal of temperature. The values of $N \equiv R_\parallel/R_\perp$ for all those spectra are nearly equal to 1, indicating that the rotational diffusion of PD–Tempone in glycerol–D_2O solvent is isotropic.

compared to the older trial-and-error procedure. We illustrate the performance of such a procedure in fig. 12 and 13 to obtain the rotational diffusion coefficients and activation energy from slow-motional EPR spectra of PD–Tempone in glycerol–water solvent.

I acknowledge the contributions of my co-workers: D. Budil, R. H. Crepeau, K. Earle, D. Gamliel, J. Gorcester, M. T. Ge, B. Lynch, G. Millhauser, J. Moscicki, B. Patyal and Y. K. Shin to the research reported here. This work was supported by NSF Grants CHE 8703014 and DMR 8901718 and by NIH Grant GM 25862.

References

1 J. Gorcester and J. H. Freed, *J. Chem. Phys.*, 1986, **85**, 5375.
2 J. Gorcester and J. H. Freed, *J. Chem. Phys.*, 1988, **88**, 4678.
3 J. Gorcester and J. H. Freed, *J. Magn. Reson.*, 1988, **78**, 291.
4 J. Gorcester, S. Rananavare and J. H. Freed, *J. Chem. Phys.*, 1989, **90**, 5764.
5 J. Gorcester, G. L. Millhauser and J. H. Freed, in *Advanced EPR; Applications in Biology and Biochemistry*, ed. A. J. Hoff (Elsevier, Amsterdam), 1989), chap. 5.
6 J. Gorcester, G. L. Millhauser and J. H. Freed, in *Modern Pulsed and Continuous-wave Electron Spin Resonance*, ed. L. Kevan and M. Bowman (Wiley, NY, 1990), chap. 3.
7 G. L. Millhauser and J. H. Freed, *J. Chem. Phys.*, 1984, **81**, 37.
8 G. L. Millhauser and J. H. Freed, *J. Chem. Phys.*, 1986, **85**, 63.
9 L. J. Schwartz, G. L. Millhauser and J. H. Freed, *Chem. Phys. Lett.*, 1986, **127**, 60.
10 G. L. Millhauser, J. Gorcester and J. H. Freed, in *Electron Magnetic Resonance of the Solid State*, ed. J. A. Weil, Can. Chem. Soc. Publ. 571 (1987).
11 W. B. Lynch, K. A. Earle and J. H. Freed, *Rev. Sci. Instr.*, 1988, **59**, 1345.
12 D. Budil, K. A. Earle, W. B. Lynch and J. H. Freed, *in Advanced EPR: Applications in Biology and Biochemistry*, ed. A. J. Hoff (Elsevier, Amsterdam, 1989), chap. 8.
13 J. P. Hornak, J. K. Moscicki, D. J. Schneider and J. H. Freed, *J. Chem. Phys.*, 1986, **84**, 3387.
14 D. A. Cleary, Y. K. Shin, D. J. Schneider and J. H. Freed, *J. Magn. Reson.*, 1988, **79**, 474.
15 J. K. Moscicki, Y. K. Shin and J. H. Freed, *J. Magn. Reson.*, 1989, **84**, 554.
16 J. K. Moscicki, Y. K. Shin and J. H. Freed, in *EPR Imaging and In Vivo EPR*, ed. G. Eaton and S. Eaton (CRC Press, Boca Raton, Fla, 1990), in press.
17 K. V. Vasavada, D. J. Schneider and J. H. Freed, *J. Chem. Phys.*, 1987, **86**, 647.

18 D. J. Schneider and J. H. Freed, *Adv. Chem. Phys.*, 1989, **73**, 387.
19 D. J. Schneider and J. H. Freed, in *Spin Labeling Theory and Applications, Biol. Magn Reson.*, ed. L. J. Berliner and J. Reuben (Plenum Press, New York, 1989), vol. 8, p. 1.
20 L. J. Schwartz, A. E. Stillman and J. H. Freed, *J. Chem. Phys.*, 1982, **77**, 5410.
21 L. Kar, G. L. Millhauser and J. H. Freed, *J. Phys. Chem.*, 1984, **88**, 3951.
22 G. A. Marg, G. L. Millhauser, P. S. Skerkev and D. S. Clark, *Ann. NY Acad. Sci.*, 1986, **469**, 253; L. Kar and M. E. Johnson and M. K. Bowman, *J. Magn. Reson.*, 1987, **75**, 397.
23 J. H. Freed, in *Rotational Dynamics of Small and Macromolecules in Liquids, Lecture Notes in Physics 293*, ed. T. Dorfmüller and R. Pecora (Springer-Verlag, Berlin, 1987), p. 89.
24 S. A. Goldman, G. V. Bruno and J. H. Freed, *J. Chem. Phys.*, 1973, **59** 3071.
25 J. H. Freed, in *Spin Labeling: Theory and Applications*, ed. L. J. Berliner (Academic Press, New York, 1976), chap. 3.
26 J. S. Hyde and L. R. Dalton, in *Spin Labeling: Theory Applications*, ed. L. J. Berliner (Academic Press, New York, 1979), vol. 2.
27 L. A. Dalton and L. R. Dalton, in *Multiple Electron Resonance Spectroscopy*, ed. M. M. Dorio and J. H. Freed (Plenum Press, New York, 1979).
28 J. P. Hornak and J. H. Freed, *Chem. Phys. Lett.*, 1983, **101**, 115.
29 S. A. Dzuba, A. G. Maryasov, K. M. Salikhov and Yu. D. Tsvetkov, *J. Magn. Reson.*, 1984, **58**, 95.
30 J. H. Freed, in *Time Domain Electron-Spin Resonance*, ed. L. Kevan and R. N. Schwartz (Wiley, New York, 1979).
31 J. S. Hyde, in ref. (30); J. S. Hyde, W. Froncisz and C. Mottley, *Chem. Phys. Lett.*, 1984, **110**, 621.
32 L. J. Schwartz, *PhD Thesis* (Cornell University, 1984).
33 M. Bowman, in *Modern Pulsed and Continuous-Wave Electron Spin Resonance*, ed. L. Kevan and M. Bowman (Wiley, New York, 1990), chap. 1.
34 R. H. Crepeau, A. Dulcic, J. Gorcester, J. R. Saarinen and J. H. Freed, *J. Magn. Reson.*, 1989, **84**, 184.
35 D. Gamliel and J. H. Freed, *J. Magn. Reson.*, 1990, **88**, in press.
36 J. Jeener, B. H. Meier, P. Bachman and R. R. Ernst, *J. Chem. Phys.*, 1983, **71**, 850.
37 O. Ya. Grinberg, A. Dubinski and Ya. S. Lebedev, *Russ. Chem. Rev.*, 1983, **52**, 850.
38 Y. K. Shin, J. K. Moscicki and J. H. Freed, *Biophys. J.*, 1990, **57**, 445.
39 A. Nayeem, S. Rananavare and V. S. S. Sastry, *J. Chem. Phys.*, 1989, **91**, 6887.
40 B. Berner and D. Kivelson, *J. Phys. Chem.*, 1979, **83**, 1406.
41 G. Moro and J. H. Freed, *J. Chem. Phys.*, 1981, **74**, 3757.
42 G. Moro and J. H. Freed, in *Large-scale Eigenvalue Problems*, ed. J. Cullum and R. Willoughby, *Mathematics Study Series 127* (North-Holland, Amsterdam, 1986), p. 143.
43 G. Moro and J. H. Freed, *J. Chem. Phys.*, 1981, **75**, 3157.
44 R. H. Crepeau, S. Rananavare and J. H. Freed, *Abs. 10th Int. EPR Symp. Rocky Mtn. Conf.*, Denver, CO, 1987.
45 J. S. Hwang, R. P. Mason, L-P. Hwang and J. H. Freed, *J. Phys. Chem.*, 1975, **79**, 489.

Paper 0/01881C; *Received* 27*th April*, 1990